Conference on Modelling Fluid Flow (CMFF'22)
The 18th International Conference on Fluid Flow Technologies
Budapest, Hungary, August 30-September 2, 2022

MODELING ELECTROHYDRODYNAMICALLY ENHANCED DRAG IN CHANNEL AND PIPE FLOWS USING ONE-DIMENSIONAL TURBULENCE

Marten KLEIN[1], Juan Alí MEDINA MÉNDEZ[1], Heiko SCHMIDT[1]

[1] Chair of Numerical Fluid and Gas Dynamics, Faculty of Mechanical Engineering, Electrical and Energy Systems, Brandenburg University of Technology (BTU) Cottbus-Senftenberg. Siemens-Halske-Ring 15A, D-03046, Cottbus, Germany. Tel.: +49 355 69-5127, Fax: +49 355 69-5127, E-mail: marten.klein@b-tu.de (M. Klein), medinjua@b-tu.de (J. A. Medina Méndez), heiko.schmidt@b-tu.de (H. Schmidt)

ABSTRACT

The joint modeling of flow hydrodynamics and electrokinetics is a relatively unexplored area of turbulent flow research. We address a lack of available models for electrohydrodynamic (EHD) turbulent flow utilizing a lower-order approach, the stochastic One-Dimensional Turbulence (ODT) model. ODT is constructed on the principles of the direct energy cascade of Navier–Stokes turbulence, with key emphasis on the accurate resolution of the small molecular transport scales within a notional line-of-sight. We investigate two canonical flow configurations to demonstrate the applicability of the model in the simulation of EHD flows. First, we investigate EHD effects in zero-pressure-gradient turbulent boundary layers by two-way coupled model application to plane Couette flow of a dilute electrolyte. Second, we apply the one-way coupled model to EHD-enhanced gas flow through a vertical pipe with an inner concentric electrode, where electric fields are generated by means of a corona discharge and the corresponding effect of a continuum ionic charge density field.

Keywords: EHD turbulence, multiphysical boundary layers, one-dimensional turbulence, stochastic modeling, turbulent drag enhancement

1. INTRODUCTION

Electrohydrodynamic (EHD) flows are encountered in various technical applications. As an overview of research-led EHD applications we cite examples of electrostatic precipitation [1], EHD-enhancement of heat and mass transfer [2, 3], turbulent drag [4], hydrogen production in water electrolysis [5], plasma-assisted combustion [6], among others. For numerical simulations of such devices, it is crucial to accurately and economically model entangled hydrodynamic and electrokinetic processes down to and even below the Kolmogorov and Batchelor scales [7]. One of the key issues for accurate modeling of EHD flows is the correct representation of nonlocal and nonlinear interactions between the fluid flow, charge-carrier distributions, and electric fields. These interactions may cause a departure of the turbulence dynamics, e.g., from K41 [8] to electrokinetic turbulence [9]. Indeed, on some EHD regimes, turbulence may appear even at very low Reynolds numbers, e.g., when the electric body forces substitute the role of external inertial forces, and the former are in a large ratio with respect to the viscous forces [10]. Direct Numerical Simulations (DNSs) should be the method of preferred choice for unraveling the physics presents in EHD flows. However, DNSs are, even to this day, limited in terms of their heavy computational overload, i.e., limited to moderate Reynolds numbers [11]. Needless to say, diffusive sub-grid-scale parameterizations used in Reynolds-averaged Navier–Stokes (RANS) or large-eddy simulations (LES), specifically in the presence of walls, are of limited applicability in EHD flows. This is because turbulent drag modifications are nonuniversal and, depending on the flow regime, related to flow laminarization or turbulence regeneration by the action of spatially varying body forces (e.g. [12, 13]) that require new modeling strategies.

Alternative to averaged and filter-based turbulence models, we address issues in turbulent EHD flows with a dimensionally reduced stochastic modeling approach, the so-called One-Dimensional Turbulence (ODT) model [14]. The model has the capability to capture detailed statistics of simultaneous scalar and momentum transport in the vicinity of a wall (e.g. [15]) and complex mixing processes in the bulk (e.g. [16]). In general, ODT aims to resolve all relevant scales of the flow but only for a one-dimensional (1-D) domain that represents a notional line-of-sight. A stochastic process is used to mimic the effects of turbulent stirring motions, whereas deterministic molecular diffusion, electric drift currents, Coulomb forces, and boundary conditions, are directly resolved. For the present standalone application to wall-bounded EHD turbulence,

the ODT domain is aligned with the wall-normal coordinate. This allows to resolve details of wall-normal transport processes and to capture variable momentum sources [16] and nonhomogeneous electric fields [17] if needed.

The rest of this paper is organized as follows. Section 2 gives an overview of the ODT model formulations for multiphysical wall-bounded flows with an extension to EHD flows. Section 3 collects key results partitioned into two-way coupled EHD Couette flow of dilute electrolytes and one-way coupled EHD-enhanced vertical pipe flow with an inner concentric electrode. Last, in Section 4, we summarize the two case studies.

2. FLOW MODEL FORMULATION

2.1. Overview of the ODT model

In decaying isotropic turbulence seen on a line-of-sight through the turbulent flow (the ODT line), piecewise-transformations on scalar profiles, or triplet maps, induce an increase in the rate of strain, which is characteristic of turbulent eddies. Symbolically, the effect of the triplet map $f(y)$ on an instantaneous profile of the property field $\psi(y)$ is denoted as the transformation $\psi(y) \rightarrow \psi(f(y))$ (in a y-oriented wall-normal domain of a Cartesian coordinate system) [14]. The triplet map microscopically models turbulence phenomenology. It takes a property profile along a selected size l interval, compresses the profile to $l/3$, pastes two copies of this profile to fill again, and flips the central copy to ensure continuity.

Such mapping events are stochastically sampled from unknown distribution functions with the aid of a Poisson process (e.g. [18]). Based on assumed distribution functions for the mapping event size l and location y_0, an efficient thinning-and-rejection method is used for probabilistic selection, in which the rate of implementation of the mappings is calculated in accordance with the local turbulence time-scale (eddy turnover time τ). The latter is obtained from the available energy of the current flow state. Under absence of body forces, the available energy follows from the velocity shear across a size-l interval around location y_0 [14] since the eddy kinetic energy, l^2/τ^2, is proportional to the squared eddy velocity, u_K^2. This scale velocity is modified when eddy-available potential energy and viscous effects are taken into account as detailed below. A factor of proportionality that controls the rate of implemented mapping events is included in the model as a rate parameter, C. The kinetic energy and the rate-of-strain are related by means of an equivalent turbulent diffusivity. The implementation of a given map at fixed turbulent diffusivity then favors the sampling of further mappings. This is the model representation of the turbulent kinetic energy cascade [14].

The set of operations comprising the sampling process and the mappings themselves is known as an eddy event. For decaying isotropic turbulence, there are still two other elements required in the model to complete a consistent dynamic picture of turbulence. One is a mechanism for viscous transport implementation, and the other one is a mechanism for turbulence kinetic energy (TKE) dissipation. Both are a consequence of the viscous momentum flux, which is implemented in a direct way in ODT, by resolving the corresponding numerical fluxes in the 1-D domain after an eddy event has been sampled [14]. This leads to the formulation of a symbolic 1-D partial differential equation (PDE) for a scalar velocity component ψ in ODT. Specialized to Cartesian coordinates in a temporal ODT formulation, this is

$$\frac{\partial \psi}{\partial t} = M - \frac{\partial F(\psi)}{\partial y}. \tag{1}$$

Here, $F(\psi)$ is the model-resolved flux of ψ, e.g., $F(\psi) = -\sigma\,(\partial\psi/\partial y)$ for molecular diffusive gradient fluxes in which σ is a kinematic diffusion coefficient. $M = M(C, y, f(y))$ represents discrete mapping effects that punctuate deterministic evolution of the conserved scalar $\psi(y, t)$ at discrete times. The mapping effects depend on the selected physical mapping $f(y)$, which models turbulent microstructure, and a turbulent eddy rate parameter C. Note that there is an alternative spatial ODT formulation, which is generally treated as a reinterpretation of the parabolic temporal ODT formulation. Details on the spatial formulation are omitted here, but these can be found in other ODT publications [19, 20, 21].

2.2. Model formulation for temporally developing planar wall-bounded flow

The presence of walls introduces a wall-normal-position dependence on the turbulent scalar transport. Close to the wall, viscous transport is dominantly one-dimensional, aligned with the wall-normal direction. Away from the wall, viscous transport may have a more inherent three-dimensional (3-D) character, although the turbulent transport may dominate instead. The transition between the near-wall and away-from-the-wall behavior is controlled in ODT in practical terms by the model parameter Z. The latter defines a viscous penalty by setting a lower limit below which eddy implementation is suppressed [22]. This imposes the dominance of the viscous transport.

Another important dynamical feature in wall-bounded flows is the anisotropy of the velocity statistics. In this context, the role of the turbulent pressure transport is the redistribution of the TKE among the Reynolds stress components [23]. In ODT, this pressure-scrambling effect is modeled with the aid of a kernel function $K(y) = y - f(y)$ [22]. Eddy events are modified to implement mappings, as well as the kernel effects for velocity components, such that $\psi(y) \rightarrow \psi(f(y))$ for a conserved scalar, and $u_i(y) \rightarrow u_i(f(y)) + c_i K(y)$ for the Cartesian velocity components u_i, $i = 1, 2, 3$. As detailed in [22], c_i is a kernel coefficient calculated based on the available energy and a model parameter $\alpha \in [0, 1]$ that controls the efficiency of inter-component kinetic energy

redistribution, such that

$$c_i = \frac{1}{\int_{y_0}^{y_0+l} \rho K^2 \,\mathrm{d}y} \Bigg(u_{i,K} + \mathrm{sgn}\left(u_{i,K}\right) \times \sqrt{(1-\alpha)\, u_{i,K}^2 + \frac{\alpha}{2}\left(u_{j,K}^2 + u_{k,K}^2\right)} \Bigg). \tag{2}$$

Here, $u_{i,K} = \int_{y_0}^{y_0+l} \rho u_i(f(y)) K(y) \,\mathrm{d}y$, where ρ is the uniform density, and (i, j, k) permutations of $(1, 2, 3)$.

The expression for τ, or in this case τ^{-2}, considering $u_{i,K}$ as the available kinetic energy for redistribution, as well as the viscous penalty factor, is based on [22],

$$\tau^{-2} = \frac{2K_0}{\int_{y_0}^{y_0+l} \rho K^2(y) \,\mathrm{d}y} \times \left(\frac{K_0 \sum_i u_{i,K}^2}{2\int_{y_0}^{y_0+l} \rho K^2(y) \,\mathrm{d}y} - \frac{Z}{2} \frac{\mu_{\mathrm{eddy}}^2}{\rho_{\mathrm{eddy}} l^2} \int_{y_0}^{y_0+l} \mathrm{d}y \right). \tag{3}$$

Here, $K_0 = \left(l^2 \int_{y_0}^{y_0+l} \mathrm{d}y \right)^{-1} \int_{y_0}^{y_0+l} K^2(y) \,\mathrm{d}y$, which converges to $4/27$ in the continuum kernel limit. Additionally, μ_{eddy} and ρ_{eddy} are weighted averages of the dynamic viscosity and the density within the eddy range $[y_0, y_0 + l]$. The density and dynamic viscosity of the fluid are assumed as constants, and of uniform value.

Eddy events are sampled in time on the basis of an acceptance probability P_a, following a Poisson process. The value of P_a for a selected candidate eddy event is calculated as in [14] based on the current flow state. Considering the rate parameter C, the acceptance probability is given by

$$P_a = C \frac{\Delta t_s}{\tau} \frac{1}{l^2 \chi(l, y_0)} < 1. \tag{4}$$

Here, Δt_s is a sampling time interval that needs to be able to resolve any possible eddy turnover time τ. Hence, we select $\Delta t_s < \tau$, which is adapted dynamically in the implementation (see [22]). Furthermore, $\chi(l, y_0)$ is a presumed joint probability density function (JPDF) of eddy event sizes and locations which is used to obtain reasonable candidate events. Oversampling and rejection guarantees that ODT simulation results are insensitive to the exact choice of this JPDF.

After an eddy event is implemented, the deterministic evolution is comparable to that in Eq. (1). With the model resolved viscous flux $F_i(u_i) = -\nu\,(\partial u_i / \partial y)$, mapping (M_i) and kernel, as well as momentum sources for the selected component i, we obtain

$$\frac{\partial u_i}{\partial t} = M_i + K_i + S_i + \nu \frac{\partial^2 u_i}{\partial y^2}. \tag{5}$$

This expression incorporates now symbolically the effects of the kernel, and of the energy redistribution among velocity components, by means of the term $K_i(C, Z, \alpha, u, f(y))$. S_i is a source term for the i-th velocity component to be integrated together with the viscous flux, e.g., a fixed pressure gradient (FPG).

2.3. Extension to spatially developing flow with variable density effects

The model formulation presented in Section 2.2 considers the temporal change of scalar profiles along a line-of-sight through the turbulent flow, and is generally referenced as T-ODT. An extension of the model to capture streamwise fluxes of spatially evolving flows (e.g., boundary-layer-type flows) has been presented in [14, 24] and is denoted by S-ODT. More importantly, [24] also present a variable-density formulation for low Mach number flows. In both variable-density T-ODT and S-ODT, a second kernel function $J(y) = |K(y)|$ is introduced in order to facilitate enforcement of physical conservation properties.

For variable-density flow, the various integral expressions above receive the mapped mass density such that $\rho \rightarrow \rho(f(y))$. In variable density T-ODT, the calculation of the available kinetic energy $u_{i,K}$ changes accordingly. The fractions $u_{i,K} \Big/ \int_{y_0}^{y_0+l} \rho K^2(y) \,\mathrm{d}y$ and $u_{i,K}^2 \Big/ \left(2\int_{y_0}^{y_0+l} \rho K^2(y) \,\mathrm{d}y\right)$ in Eqs. (2) and (3), change to $P_i/(2S)$ or $P_i^2/(4S)$, respectively, where, as in [24],

$$P_i = u_{i,K} - H \int_{y_0}^{y_0+l} [\rho u_i](f(y))\, J(y) \,\mathrm{d}y, \tag{6}$$

$$S = \frac{H^2+1}{2} \int_{y_0}^{y_0+l} \rho(f(y))\, K^2(y) \,\mathrm{d}y - H \int_{y_0}^{y_0+l} \rho(f(y))\, J(y)\, K(y) \,\mathrm{d}y, \tag{7}$$

$$H = \frac{\int_{y_0}^{y_0+l} \rho(f(y))\, K(y) \,\mathrm{d}y}{\int_{y_0}^{y_0+l} \rho(f(y))\, J(y) \,\mathrm{d}y}. \tag{8}$$

In the S-ODT model, the streamwise change of the scalar profiles in the line-of-sight through turbulence is studied. Two variants arise in this case. One is the conservative boundary-layer formulation [24], and another the non-conservative wall-constrained internal-flow formulation [20]. Essentially, in S-ODT, all integrals in Eqs. (6–8), as well as the integrand of $\int_{y_0}^{y_0+l} \rho K^2(y) \,\mathrm{d}y$ in the prefactor in Eq. (3), receive an additional multiplication by $u(f(y))$, the mapped streamwise advecting velocity (see [20, 24] for details). The time-scale τ changes to a streamwise length-scale ξ, and the temporal sampling Δt_s changes to a streamwise sampling Δx_s [24]. Symbolically, the S-ODT equivalent of Eq. (5) has a modified left-hand side and reads

$$u \frac{\partial u_i}{\partial x} = M_i + K_i + S_i + \nu \frac{\partial^2 u_i}{\partial y^2}. \tag{9}$$

2.4. Extensions to cylindrical geometry

An additional model extension, or a generalization of the T-ODT and S-ODT formulations for both Cartesian and cylindrical flows, considering a dynamically adaptive mesh, was presented in [19]. The cylindrical formulation replaces the planar coordinate y for the radial coordinate r, while any line-integral $\int(\cdot)\,\mathrm{d}y$ in all of the equations presented so far, changes to a surface radial integral of the form $\int(\cdot)\,r\,\mathrm{d}r$. Eqs. (1) and (9) also consider a change in the form of the gradient flux. The generalized scalar conservation equation, Eq. (1), becomes

$$\frac{\partial\psi}{\partial t} = M(C,Z,r,f(r)) - \frac{1}{r}\frac{\partial\left(rF(\psi)\right)}{\partial r}, \tag{10}$$

where $F(\psi) = -\sigma\,(\partial\psi/\partial r)$ for the model resolved radial molecular diffusive flux. The specific form of the viscous flux for every velocity component in the cylindrical coordinate system is given in [20].

Note that [20] also introduces a variable-density formulation in which the density is treated as an active scalar, coupled with the evolution of the temperature. The temperature and density states are coupled by the ideal gas law and the divergence condition during the deterministic evolution between subsequent eddy events. This procedure is the equivalent of the enforcement of mass and energy conservation.

2.5. Incorporation of EHD effects

Incorporation of EHD effects is done by the implementation of an appropriate form of the Coulomb forces and by the account of the change in electrostatic potential energy in the ODT eddy sampling procedure. The Coulomb force density is given by $\rho_f E_i$, which is a body force that can be implemented in the ODT momentum equations, e.g., Eq. (9) (in such case, per unit mass density of the fluid). Here, $\rho_f = e(n_+c_+ - n_-c_-)$, is the continuum density of free charges due to positively (+) and negatively (−) charged scalars (i.e., electrochemical species or tracers) with concentration $c_\pm$ and valence $n_\pm$ multiplying the unit charge e on an electron, and by Faraday's law for nonmagnetic media, the electric field is given by $E_i = -\partial\Phi/\partial x_i$, where Φ denotes the total electrostatic potential and $(x_i) = (x,y,z)^{\mathrm{T}}$ the Cartesian coordinates. The concentrations $c_\pm$ obey individual scalar conservation equations similar to Eq. (1), but also other formulations specializing to electron an ion currents are possible. Coulomb forces acting perpendicular to the ODT line are treated straightforwardly as momentum sources [17] that drive turbulence by an increase of velocity shear, whereas those acting along the ODT line affect the eddy rate analogous to gravity [14, 25] as detailed below.

The main goal for the present application cases is capturing leading-order EHD effects that are associated with a modification of the boundary-layer dynamics. Hence, the developed 'minimal flow model' shall be able to capture wall-normal contributions to nonuniversal EHD turbulence circumventing computation of 3-D electric fields. For the stand-alone ODT application to EHD channel and pipe flows considered here, it is assumed that all property fields are not only statistically but also momentarily approximately homogeneous in the lateral directions. Available reference DNS [4] indicate that this assumption is reasonable for the background mean state justifying application to cases with weak fluctuations.

The transfer of electrostatic potential energy to kinetic energy of the flow, or *vice versa*, is the mechanism for implementation of the effects of the work performed by the flow against Coulomb forces by a notional eddy turnover, represented as the instantaneous application of the triplet map $f(y)$ for the wall-normal coordinate y. For the application cases analyzed here, only the effects of a resolved electric field along the ODT line are considered, thus any electrostatic potential energy involved in the formulation is due to the resolved E_2 component of the electric field. Non-resolved components E_1 and E_3, that are zero on average for the cases at hand, are neglected. In that sense, there is no *direct* contribution to the mean kinetic energy by $\rho_f E_i$, given that the modeled effect is simply seen as a modification of the pressure gradient in the line direction. Any EHD-enhancement (or loss), is then a consequence of a modified fluctuating pressure transport, which is modeled in ODT by the kernel kinetic energy redistribution. This is the formulation equivalent of a modification in the Reynolds stress tensor components, which is conceptually comparable to the discussion in [26] on the effect of electric body forces.

The form of the change in electrostatic potential energy, ΔE_{pot}, results from the work performed on the fluid due to the energy release from the pre-mapped to the post-mapped state analogous to buoyancy [14, 25]. ΔE_{pot} has to be added within the square bracket of Eq. (3) for EHD-enhanced sampling. Likewise, it requires a multiplication by $4S$ under the square root of Eq. (2) for potential energy redistribution due to the ODT kernel. Specializing to Cartesian coordinates, we have

$$\Delta E_{\mathrm{pot}} = -\int_{y_0}^{y_0+l} \Big[\rho_f(f(y))\,\Phi(\rho_f(f(y))) - \rho_f(y)\,\Phi(\rho_f(y))\Big]\,\mathrm{d}y. \tag{11}$$

In addition to this equation and the solution of Eq. (5), the 1-D conservation equation for ρ_f, and the Nernst–Planck equation, are solved together with the 1-D representation of Gauss' law for the electric potential, $\partial(\epsilon E_i)/\partial x_i = \rho_f$, as well as Faraday's law, $E_i = -\partial\Phi/\partial x_i$, for a known electric permittivity ϵ and the dynamically resolved component $i = 2$, which is acting along the ODT line and energetically influences turbulent eddy implementations.

The above considerations yield two different types of EHD coupling. In the one-way coupling case, the Nernst–Planck equation reduces to a zero-

divergence condition for the electric current density [27]. This results then in a uniform electric current density along the ODT line (planar Cartesian case). Electroquasistatic fields are calculated before hand and remain fixed during the simulation. In the case of two-way coupling, the Nernst–Planck equations are similar to Eq. (1). An explicit numerical solver is used in which the model resolved instantaneous profile of $\Phi(y)$ is obtained by numerical solution of a 1-D Poisson equation by application of the Thomas algorithm whenever $\rho_f(y)$ has changed.

3. RESULTS

Turbulent electroconvection exhibits different flow regimes that may be categorized by the relative strengths of the Coulomb, viscous, and inertial forces. In addition, the relaxation processes of free electric charges and their coupling to electric fields within the working fluid need to be taken into account. Typical applications are heat transfer enhancement (e.g. [3]) due to weak coupling and flow control (e.g. [4]) due to strong coupling. Below, we begin with the strongly coupled regime for plane Couette flow of a dilute electrolyte. After that, we turn to the weakly coupled regime for vertical pipe flow with an inner concentric electrode.

3.1. Drag enhancement in turbulent EHD Couette flow

In this section we consider a simple model for strongly coupled wall-bounded EHD turbulence in a Couette-type flow of a dilute electrolyte. The flow configuration is sketched in Figure 1 and corresponds with that in [4]. The top wall is moving and held at a different voltage relative to the bottom one. No-slip isopotential zero-flux wall-boundary conditions are prescribed. The T-ODT model set-up uses $C = 10$, $Z = 600$, $\alpha = 2/3$ as in [28]. The electrolytes considered have neutral bulk charge and consist of two identical ionic scalar species $\psi = c_\pm$ with the same valence and mobility but opposite charge. The model-resolved deterministic ion fluxes in accordance with Eq. (1) thus have diffusive and drift contributions so that

$$F_\pm(c_\pm) = -D\frac{\partial c_\pm}{\partial y} \mp \frac{Dc_\pm}{V_T}\frac{\partial \Phi}{\partial y}. \tag{12}$$

In analogy to [4], scaling of the Poisson–Nernst–Planck and Navier–Stokes equations (or the dimensionally reduced ODT representation of them) yields five dimensionless control parameters that define the flow state: the bulk Reynolds number, $\mathrm{Re} = Uh/\nu$, the ionic Schmidt number, $\mathrm{Sc} = \nu/D$, the dimensionless voltage, $\hat{V} = 2V/V_T$, which is varied across the range 0–40, the fixed coupling constant, $\beta = \epsilon V_T^2/(\rho\nu D) = 0.5$, and the fixed normalized Debye layer thickness, $\lambda_D/h = \sqrt{\epsilon V_T/(2\rho c_0 e h^2)} = 0.01$. In these expressions, U denotes the prescribed wall velocity magnitude, h the channel half-height, $V_T = k_B T/e$ the thermal voltage, D the kinematic diffusivity of the ions in the electrolyte, and c_0 the uniform initial concentration of the univalent ion species, respectively, in addition to the other physical parameters introduced above.

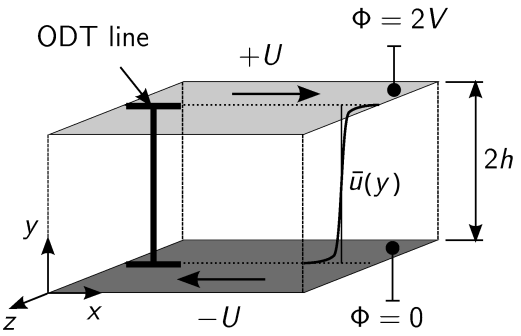

Figure 1. Sketch of the EHD Couette configuration with temporally developing flow. The one-dimensional computational domain (ODT line) is fixed in space and approximately taken as closed system in order to facilitate utilization of ODT as stand-alone tool.

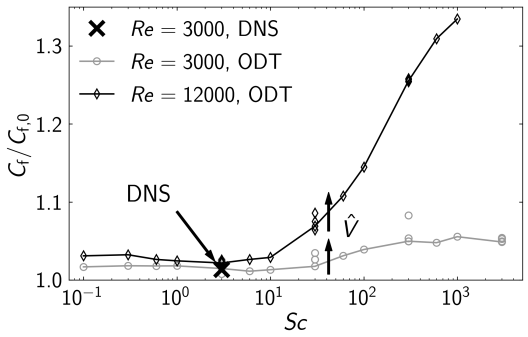

Figure 2. ODT prediction of the turbulent drag enhancement as function of Sc for various Re and $\hat{V}$ for fixed $\beta = 0.5$ and $\lambda_D/h = 0.01$, as well as fixed ODT model parameters. Connected symbols are for $\hat{V} = 10$. For fixed Sc, the drad increases with $\hat{V}$ (arrows). Reference DNS (×) is from [4].

Note that Re is the only direct control parameter for the flow regime. $\hat{V}$ is an additional control parameter that parameterizes the internal energy and thus takes the role of an equation of state. The three remaining parameters are related to the electrolyte: Sc gives the ratio of the viscous and scalar (ionic) diffusion coefficients; λ_D/h is a relative measure of electric charge separation that also determines the electric and ionic layers at the electrodes; and β expresses the strength of typical Coulomb forces in units of typical viscous forces. In a concentrated (dilute) ionic liquid (e.g. [29]), dielectric polarization is strong (weak) so that the dielectric permittivity is large (small). For constant electric charge on the ions, the Debye length has to increase (decrease) with β so that we do not consider β a variable control parameter. Instead it is kept fixed at $\beta = 0.5$ [4].

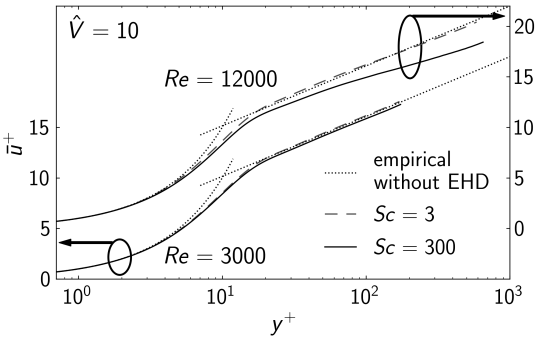

Figure 3. Dimensionless mean velocity defect $\bar{u}^+(y^+)$ for various Re **(vertically shifted) and** Sc **with $\hat{V} = 10$, $\beta = 0.5$, $\lambda_D/h = 0.01$, and fixed ODT model parameters. The empirical law of the wall (dotted; see, e.g., [32]) for hydrodynamic flow without EHD effects is given for orientation.**

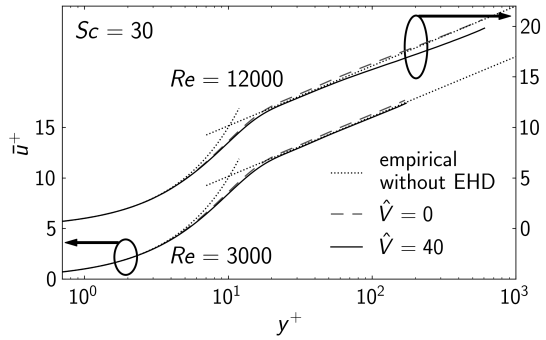

Figure 4. Dimensionless mean velocity defect $\bar{u}^+(y^+)$ for various Re **(vertically shifted) and $\hat{V}$ with** Sc = 30 **analogous to Fig. 3.**

Figure 2 shows the skin friction drag coefficient C_f, which is, for Couette flow, evaluated based on the Reynolds-averaged streamwise velocity profile, $\bar{u}(y) = \overline{u(y,t)}$, as

$$C_f = 2\frac{u_\tau^2}{U^2} \quad \text{with} \quad u_\tau = \sqrt{\nu \left|\frac{\mathrm{d}\bar{u}}{\mathrm{d}y}\right|_{\text{wall}}}. \tag{13}$$

ODT pre-simulations conducted for $\hat{V} = 0$ (absence of EHD effects; not shown here) agree with corresponding purely hydrodynamic reference experiments [30] within 2–5% yielding $C_{f,0} \approx 5.9 \times 10^{-3}$ for Re = 3000 and $C_{f,0} \approx 4.7 \times 10^{-3}$ for Re = 12,000, respectively. This level of agreement is also exhibited by the EHD-enhanced cases at Sc $\simeq$ 1 that only mildly overestimate available reference DNS as shown in Fig. 2. In fact, present ODT results suggest that the turbulent drag is largely insensitive to EHD effects for Sc $\lesssim$ 10.

A significant increase of the turbulent drag can be seen in Fig. 2 for Sc $\gtrsim$ 30 up to $\approx$ 30% for Sc $\geq$ 300 at Re = 12,000 investigated. The magnitude of the effect increases with Sc, Re, and $\hat{V}$. Interestingly, ODT predicts a regime change for the critical Schmidt number $\mathrm{Sc}_{\mathrm{crit}} \simeq 30$, which agrees with an inferred value of $\mathrm{Sc}_{\mathrm{crit}} \sim O(10)$ suggested by [4] based on DNS, albeit it remained elusive if drag increases or decreases due to enhanced coupling. In any case, the ODT prediction suggests that Re must be large enough so that the turbulent scaling cascade is broad enough to be sensibly influenced by EHD effects [31].

Figures 3 and 4 show wall-normal profiles of the dimensionless mean velocity deficit $\bar{u}^+$ over the dimensionless boundary layer coordinate y^+ given by

$$\bar{u}^+ = \frac{|\bar{u} - u_{\text{wall}}|}{u_\tau}, \quad y^+ = \frac{y u_\tau}{\nu}. \tag{14}$$

ODT simulation results are shown for various Re, Sc, and $\hat{V}$ in order to assess which region of the boundary layer is influenced by EHD effects. The hydrodynamic law of the wall (e.g. [32]) is given for orientation for the intersecting viscous sub and log layers, $\bar{u}^+(y^+) = y^+$ for $y^+ < 5$ and $\bar{u}^+(y^+) = \kappa^{-1} \ln y^+ + B$ with $\kappa = 0.39$ and $B = 4.2$ for $y^+ > 30$, respectively. ODT results for $\hat{V} = 0$ (without EHD effects) reproduce the sub and log layer exactly, though with some deficit in the buffer layer at around $y^+ \simeq 30$ when compared with reference data [4] (not shown here for clarity). For finite $\hat{V} \gtrsim O(10)$, boundary layer similarity is broken first in the bulk and outer layer for the ODT simulations with Re = 12,000 and Sc = 30. For further increasing Sc or $\hat{V}$, the entire log region is affected while near-wall similarity is exactly maintained for $y^+ < 10$ and approximately maintained for $10 < y^+ < 100$. Decreasing $\bar{u}^+$ for increasing Sc or $\hat{V}$ reflects the increase in u_τ due to which C_f increases so that the trends in Figs. 3 and 4 are consistent with those in Fig. 2.

Altogether, the results obtained demonstrate that ODT is a lower-order but high-fidelity flow model that is able to predict sensible mean effects in two-way coupled EHD turbulence for at least moderately high Re and Sc. This regime is presently inaccessible to DNS and not faithfully treatable with LES or RANS due to the inapplicability of modeling assumptions involved. A 3-D extension of the stochastic model (e.g., based on ODTLES [33, 34] or AME [35]) and dedicated reference experiments are needed in order to asses the 1-D model prediction in order to clarify its applicability to EHD turbulence.

3.2. Drag enhancement in turbulent EHD vertical pipe flow

In this section we present the results for a one-way coupled EHD pipe flow simulation with an inner concentric electrode, which resembles the experimental electrostatic precipitator (ESP) device of [36]. In the following, we slightly extend a recent comprehensive ODT study [21] on pipe flow ESP, which was conducted by two of the authors and that addresses the application case and modeling in more detail.

A sketch of the flow configuration is shown in

Figure 5. In the ODT simulations, the radially oriented S-ODT line is advected upwards with the flow through the ESP, i.e., this is a spatial ODT formulation. The cylindrical pipe flow is subject to an electric field induced by a (positive) corona discharge originated at the electrode. We only consider one-way coupled electric fields which are not modified by fluctuations in ρ_f, yet equally affect the stochastic random sampling as described in Sec. 2.5. Electric charges (positive ions in air) are assumed as a continuum phase. For details on the generation of the electroquasistatic (EQS) fields and on the general implementation, please refer to [21] or [37]. In addition to the electrostatic potential energy formulation used during eddy events, we also incorporate the Joule heating as a source term to resolve during the deterministic advancement of the temperature equation, see [21, 37].

The objective of the simulations is the evaluation of the friction drag, which is represented in [36] by the Darcy friction factor,

$$f_D = -\frac{4R}{\rho_b U_b^2}\frac{\mathrm{d}\overline{p}}{\mathrm{d}z}, \tag{15}$$

where R is the outer radius of the cylindrical pipe ESP. The mean flow is axially symmetric due to geometry. Hence, $\mathrm{d}\overline{p}/\mathrm{d}z$ can be obtained from the Reynolds-averaged momentum equations, neglecting turbulent correlations of the molecular dynamic viscosity. Indeed, the wall pressure difference, between the outlet and the inlet of a pipe section of finite length Δ, can be calculated as

$$\begin{aligned}\Delta p_w = &\\ &-\frac{2}{R^2}\Delta\left(\int_0^R \langle\rho u_1 u_1\rangle\, r\,\mathrm{d}r - R^2\left(\langle\mu\rangle\frac{\partial\langle u_2\rangle}{\partial r}\right)\Big|_R\right)\\ &-\frac{2}{R^2}\Delta\left(\int_0^R \langle\mu\rangle\frac{\partial\langle u_2\rangle}{\partial r}\, r\,\mathrm{d}r\right) - \frac{2}{R}\int_0^{B_{\mathrm{TS}}}\tau_w \mathrm{d}z\\ &-\frac{J_R}{\beta_f},\end{aligned} \tag{16}$$

where Δ refers to a difference between the location of the outlet (i.e., $z = B_{\mathrm{TS}}$) and the inlet (i.e., $z = 0$) of the simulated device. J_R is the uniform radially weighted electric current density, which is obtained from the voltage-current values given as an input to the simulation, and β_f is the mobility of the free ionic charges. Eq. (16) allows an approximation of the average pressure gradient required for Eq. (15) as $\mathrm{d}\overline{p}/\mathrm{d}z \approx \Delta p_w / B_{\mathrm{TS}}$.

Figure 6 shows the ensemble average of the inlet profiles used in the S-ODT simulations. Two different types of profiles are used based on the geometry of the experimental device. Unlike a traditional pipe flow, the configuration in Fig. 5 includes an internal electrode boundary, which imposes a no-slip condition at the electrode. Note that the sketch provided in Fig. 5 corresponds to the test section of the experimental device, see [36]. The device possesses an entry section, which is supposed to provide

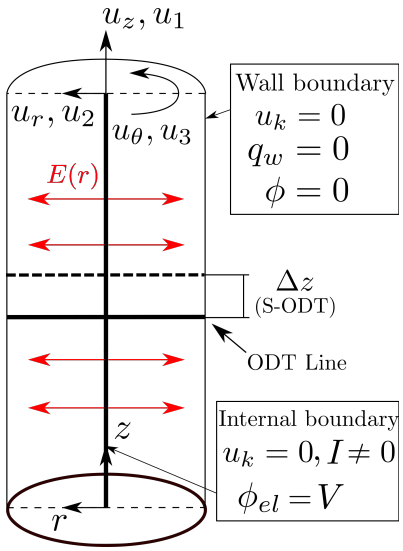

Figure 5. Sketch of the spatially developing EHD vertical pipe flow. The ODT line is advected upwards with the momentary axial velocity during a simulation run. $I \neq 0$ refers to the electrical current needed to inject charge carriers at the axis by a corona discharge.

a fully developing flow at the inlet of the test section. However, a verification of the hydrodynamic entry length L_H (see [39]) performed for one of the Reynolds number cases in [36], $\mathrm{Re}_b = 4000$, shows that L_H is larger than the sum of both device entry and test section lengths. Therefore, we evaluate both fully developed turbulent inlet profiles (generated with a cylindrical T-ODT formulation), as well as equivalent turbulent flow profiles achieving a target developing f_D value. The latter is calculated according to the actual entry and test section lengths, and the formula provided in [39].

Figure 7 shows the results for the evaluation of f_D. The experimental device has radius $R = 1.6 \times 10^{-2}$ m, test section length $B_{\mathrm{TS}} = 1.02$ m, and entry section length $B_{\mathrm{entry}} = 1.59$ m. The inner concentric electrode of the device has radius $R_{\mathrm{elec}} = 1.25 \times 10^{-4}$ m, and length $B_{\mathrm{elec}} = 2.05$ m. The inlet gas flow is assumed at atmospheric pressure with uniform fluid properties (Prandtl number $\mathrm{Pr}_{\mathrm{air}} \simeq 0.71$) at a temperature $T_0 = 300.15$ K. The inlet flow has a bulk velocity $U_b = 2$ m/s, and associated $\mathrm{Re}_b = 4000$. We evaluate three different Masuda numbers: $\mathrm{Md} \approx 1.97 \times 10^4$, 1.27×10^5, and 3.17×10^5, on top of the neutral (no EHD) pipe flow condition. The Masuda number (e.g. [40, 41]) is here defined as $\mathrm{Md} = \epsilon_0\, \Phi_{\mathrm{el}}\, (\Phi_{\mathrm{el}} - \Phi_{\mathrm{on}}) \,/\, (\rho_0 \nu_0^2)$, where ϵ_0 is the vacuum electrical permittivity, ρ_0 and ν_0 the reference mass density and kinematic viscosity of the gas, respectively, $\Phi_{\mathrm{el}} = V$ the electrode operating voltage, and Φ_{on} the corona-discharge onset voltage (both voltages are measured in the experiments) relative to the grounded pipe with voltage $\Phi_{\mathrm{pipe}} = 0$.

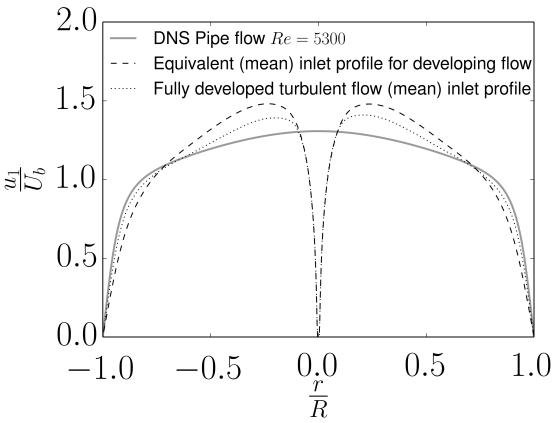

Figure 6. Ensemble average of initial (inlet) conditions for the evaluated Re = 4000 **pipe flow (see description in text). The reference DNS is from [38] and shown for comparison.**

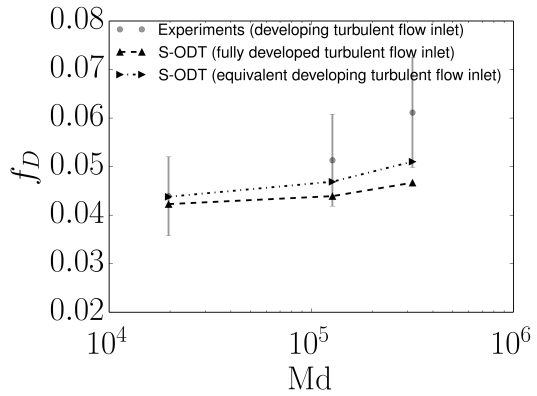

Figure 7. ODT prediction of the enhancement of the Darcy friction factor f_D with the dimensionless EHD body force (Masuda number Md**). Reference experiments are from [36].**

Despite the friction factor evaluation being simply an integral quantity of the flow, the results obtained by the ODT simulations (see Fig. 7) are worth commenting due to the multiphysical nature of the application. This is neither an application that can be easily evaluated by DNS nor treated faithfully with LES or RANS. ODT provides small-scale resolution and dynamical complexity by capturing relevant physical processes at feasible cost. The relative contributions to the pressure gradient according to Eq. (16) are thus model predictions. It has been verified that the largest contribution to $\mathrm{d}\overline{p}/\mathrm{d}z$ is due to the wall shear stress τ_w, and in second place, by the average kinetic energy gradient. The latter is the reason why the utilization of developing flow inlet conditions are necessary to obtain a model prediction that reasonably captures the reference experiments.

4. SUMMARY

EHD turbulence denotes a chaotic flow that is influenced by inertial, viscous, and Coulomb forces across a range of scales. Dynamical processes are nonuniversal and reach down to the Kolmogorov scale [8], η_K, and Batchelor scales [42], $\mathrm{Sc}^{-1/2}\eta_K$, placing a strong burden on numerical simulation and modeling. For EHD turbulence it has been shown recently that the smallest scales for the flow kinetic energy and, hence, also high-Sc transported scalars are not the Kolmogorov and Batchelor scales, but new characteristic EHD scales [7, 13]. These emerging scales can be even smaller than the Kolmogorov and Batchelor scale increasing the cost of numerical simulation of EHD turbulence. In applications, like membraneless redox flow [43] and liquid metal [44] batteries, but alao in wire-plate precipitators [17], EHD flows are confined so that velocity and scalar boundary layers, in particular Debye layers, at domain walls and internal interfaces have to be resolved. Resolution and predictability requirements are addressed here by utilizing the stochastic One-Dimensional Turbulence (ODT) model for regime-overreaching numerical investigation of wall-bounded EHD-enhanced flows.

For two-way coupled EHD Couette flow, ODT predicts EHD-enhanced outer layer turbulence that nonlocally affects the entire turbulent boundary layer. Turbulent drag increases for $\mathrm{Re} \gtrsim 10^4$ and $\mathrm{Sc} \gtrsim 30$ suggesting that charge carriers have to be immobile enough to get stirred down to the turbulent microscales in order to yield strong interactions between hydrodynamics and electrokinetics. Present ODT results suggest that at least $\sqrt{\mathrm{Sc}} \gtrsim 5$ (based on the Batchelor scale) times smaller length scales are needed in the transported electric scalar than in the velocity field.

In one-way coupled vertical EHD pipe flow with a coaxial central electrode, ODT hints at transient effects in a developing turbulent flow. Turbulent drag is enhanced by an EHD-based amplification of the rate of change of the turbulent kinetic energy as revealed by an analysis of the contributions to the pressure drop per unit pipe length. Based on boundary-layer similarity, we assert that the mechanism is at work for the radial direction in the EHD gas-phase pipe flow is similar to that in EHD Couette flow of an ionic liquid.

Altogether, ODT is a self-contained, dimensionally reduced flow model that combines fidelity, predictability, and numerical efficiency. We have demonstrated its applicability to EHD-enhanced flows for future application as sub-filter-scale model.

ACKNOWLEDGEMENTS

H.S., J.M., and M.K. acknowledge support by the European Regional Development Fund (EFRE), Grant no. StaF 23035000. Furthermore, M.K. acknowledges support by the BTU Graduate Research School (Conference Travel Grant).

REFERENCES

[1] Robinson, M., 1968, "Turbulent Gas Flow and Electrostatic Precipitation", *J Air Pollut Control Assoc*, Vol. 18 (4), pp. 235–239.

[2] Laohalertdecha, S., Naphon, P., and Wongwises, S., 2007, "A review of electrohydrodynamic enhancement of heat transfer", *Renewable Sustainable Energy Rev*, Vol. 11 (5), pp. 858–876.

[3] Bacher, C., and Riebel, U., 2021, "Electrohydrodynamically enhanced mass transfer in a wetted-wall column", *Chem Eng Res Des*, Vol. 167, pp. 183–197.

[4] Ostilla-Mónico, R., and Lee, A. A., 2017, "Controlling turbulent drag across electrolytes using electric fields", *Faraday Discuss*, Vol. 199, pp. 159–173.

[5] Shiva Kumar, S., and Himabindu, V., 2019, "Hydrogen production by PEM water electrolysis – A review", *Mater Sci Energy Technol*, Vol. 2 (3), pp. 442–454.

[6] Ju, Y., and Sun, W., 2015, "Plasma assisted combustion: Dynamics and chemistry", *Prog Energy Combust Sci*, Vol. 48, pp. 21–83.

[7] Zhao, W., and Wang, G., 2019, "Cascade of turbulent energy and scalar variance in DC electrokinetic turbulence", *Physica D: Nonlin Phen*, Vol. 399, pp. 42–50.

[8] Kolmogorov, A. N., 1941, "The local structure of turbulence in incompressible viscous fluid for very large Reynolds numbers", *Dok Akademii Nauk SSSR*, Vol. 30, pp. 299–303.

[9] Zhao, W., and Wang, G., 2017, "Scaling of velocity and scalar structure functions in AC electrokinetic turbulence", *Phys Rev E*, Vol. 95 (2), 023111.

[10] Storey, B. D., 2005, "Direct numerical simulation of electrohydrodynamic flow instabilities in microchannels", *Phys D: Nonlin Phen*, Vol. 211 (1), pp. 151–167.

[11] Duraisamy, K., Iaccarino, G., and Xiao, H., 2019, "Turbulence Modeling in the Age of Data", *Annu Rev Fluid Mech*, Vol. 51 (1), pp. 357–377.

[12] Pandey, S., Chu, X., Weigand, B., Laurien, E., and Schumacher, J., 2020, "Relaminarized and recovered turbulence under nonuniform body forces", *Phys Rev Fluids*, Vol. 5, p. 104604.

[13] Zhao, W., and Wang, G., 2021, "A tentative study of the transport of energy and other scalar quantities in forced turbulence driven by $\nabla^n A$-type volume forces", *J Hydrodyn*, Vol. 33 (6), pp. 1271–1281.

[14] Kerstein, A. R., 1999, "One-dimensional turbulence: Model formulation and application to homogeneous turbulence, shear flows, and buoyant stratified flows", *J Fluid Mech*, Vol. 392, pp. 277–334.

[15] Klein, M., Schmidt, H., and Lignell, D. O., 2022, "Stochastic modeling of surface scalar-flux fluctuations in turbulent channel flow using one-dimensional turbulence", *Int J Heat Fluid Flow*, Vol. 93, 108889.

[16] Klein, M., Zenker, C., and Schmidt, H., 2019, "Small-scale resolving simulations of the turbulent mixing in confined planar jets using one-dimensional turbulence", *Chem Eng Sci*, Vol. 204, pp. 186–202.

[17] Medina Méndez, J. A., Schmidt, H., and Riebel, U., 2019, "Towards a one-dimensional turbulence approach for electrohydrodynamic flows", *11th Int. Symp. Turbul. Shear Flow Phen. (TSFP11)*, Southampton, UK, pp. 1–6, ID 265.

[18] Papoulis, A., and Pillai, S. U., 2002, *Probability, Random Variables, and Stochastic Processes*, McGraw-Hill, New York, 4th edn.

[19] Lignell, D., Lansinger, V. B., Medina Méndez, J. A., Klein, M., Kerstein, A. R., Schmidt, H., Fistler, M., and Oevermann, M., 2018, "One-dimensional turbulence modeling for cylindrical and spherical flows: model formulation and application", *Theor Comput Fluid Dyn*, Vol. 32 (4), pp. 495–520.

[20] Medina Méndez, J. A., Klein, M., and Schmidt, H., 2019, "One-Dimensional Turbulence investigation of variable density effects due to heat transfer in a low Mach number internal air flow", *Int J Heat Fluid Flow*, Vol. 80, 108481.

[21] Medina Méndez, J. A., Bacher, C., Riebel, U., and Schmidt, H., 2022, "Electrohydrodynamically-enhanced drag in a vertical pipe-flow with a concentric electrode: A One-Dimensional Turbulence study", *European Journal of Mechanics – B/Fluids*, Vol. 95, pp. 240–251.

[22] Kerstein, A. R., Ashurst, W. T., Wunsch, S., and Nilsen, V., 2001, "One-dimensional turbulence: Vector formulation and application to free-shear flows", *J Fluid Mech*, Vol. 447, pp. 85–109.

[23] Lee, K., Venugopal, V., and Girimaji, S. S., 2016, "Pressure-strain energy redistribution in compressible turbulence: Return-to-isotropy versus kinetic-potential energy equipartition", *Phys Scr*, Vol. 91 (8), 084006.

[24] Ashurst, W. T., and Kerstein, A. R., 2005, "One-dimensional turbulence: Variable-density formulation and application to mixing layers", *Phys Fluids*, Vol. 17 (2), 025107.

[25] Wunsch, S., and Kerstein, A. R., 2005, "A stochastic model for high-Rayleigh-number convection", *J Fluid Mech*, Vol. 528, pp. 173–205.

[26] Davidson, J. H., and Shaughnessy, E. J., 1986, "Turbulence generation by electric body forces", *Exp Fluids*, Vol. 4 (1), pp. 17–26.

[27] Melcher, J. R., 1981, *Continuum electromechanics*, Vol. 2, MIT press Cambridge.

[28] Klein, M., and Schmidt, H., 2020, "Towards a stochastic model for electrohydrodynamic turbulence with application to electrolytes", *Proc Appl Math Mech*, Vol. 20, e202000128.

[29] Lee, A. A., Vella, D., Perkin, S., and Goriely, A., 2015, "Are room-temperature ionic liquids dilute electrolytes?", *J Phys Chem Lett*, Vol. 6 (1), pp. 159–163, pMID: 26263105.

[30] Robertson, J. M., 1959, "On turbulent plane Couette flow", *Sixth Midwestern Conference on Fluid Mechanics*, University of Texas, Austin, pp. 169–182.

[31] Klein, M., and Schmidt, H., 2021, "Investigating Schmidt number effects in turbulent electroconvection using one-dimensional turbulence", *Proc Appl Math Mech*, Vol. 21, e202100147.

[32] Pope, S. B., 2000, *Turbulent Flows*, Cambridge University Press, ISBN 978-0521598866.

[33] Gonzalez-Juez, E., Schmidt, R. C., and Kerstein, A. R., 2011, "ODTLES simulations of wall-bounded flows", *Phys Fluids*, Vol. 23, p. 125102.

[34] Glawe, C., Medina M., J. A., and Schmidt, H., 2018, "IMEX based multi-scale time advancement in ODTLES", *Z Angew Math Mech*, Vol. 98, pp. 1907–1923.

[35] Kerstein, A. R., 2022, "Reduced numerical modeling of turbulent flow with fully resolved time advancement. Part 1. Theory and physical interpretation", *Fluids*, Vol. 7 (2), 76.

[36] Nelson, D. A., Ohadi, M. M., Zia, S., and Whipple, R. L., 1990, "Electrostatic effects on pressure drop in tube flows", *Int J Heat Fluid Flow*, Vol. 11 (4), pp. 298–302.

[37] Medina Mendez, J. A., 2020, "Application of the One-Dimensional Turbulence model to electrohydrodynamically enhanced internally forced convective flows", Ph.D. thesis, Brandenburgische Technische Universität Cottbus-Senftenberg, Cottbus, Germny.

[38] Khoury, G. K. E., Schlatter, P., Noorani, A., Fischer, P. F., Brethouwer, G., and Johansson, A. V., 2013, "Direct Numerical Simulation of Turbulent Pipe Flow at Moderately High Reynolds Numbers", *Flow, Turbul Comb*, Vol. 91 (3), pp. 475–495.

[39] Abraham, J. P., Sparrow, E. M., and Tong, J. C. K., 2008, "Breakdown of Laminar Pipe Flow into Transitional Intermittency and Subsequent Attainment of Fully Developed Intermittent or Turbulent Flow", *Numer Heat Transfer, Part B*, Vol. 54 (2), pp. 103–115.

[40] Masuda, S., and Matsumoto, Y., 1974, "Motion of a microcharge particle within electrohydrodynamic field", *Elect Eng Jpn*, Vol. 94 (6), pp. 20–26.

[41] Masuda, S., and Hosokawa, S., 1995, "Electrostatic precipitation", J.-S. Chang, A. Kelly, and J. Crowley (eds.), *Handbook of electrostatic processes*, Marcel Dekker New York, pp. 441–480.

[42] Batchelor, G. K., 1959, "Small-scale variation of convected quantities like temperature in turbulent fluid. Part 1. General discussion and the case of small conductivity", *J Fluid Mech*, Vol. 5, pp. 113–133.

[43] Ruiz-Martín, D., Moreno-Boza, D., Marcilla, R., Vera, M., and Sánchez-Sanz, M., 2022, "Mathematical modelling of a membrane-less redox flow battery based on immiscible electrolytes", *Appl Math Model*, Vol. 101, pp. 96–110.

[44] Kolesnichenko, I., Frick, P., Eltishchev, V., Mandrykin, S., and Stefani, F., 2020, "Evolution of a strong electrovortex flow in a cylindrical cell", *Phys Rev Fluids*, Vol. 5, p. 123703.